Macromolecules

Article

pubs.acs.org/Macromolecules

Mediated Competitive Hydrogen Bonding Form Mesoporous Phenolic Resins Templated by Poly(ethylene oxide-*b*-ε-caprolactone-*b*-L-lactide) Triblock Copolymers

Chu-Chian Liu, Wei-Cheng Chu, Jheng-Guang Li, and Shiao-Wei Kuo*

Department of Materials and Optoelectronic Science, Center for Functional Polymers and Supramolecular Materials, National Sun Yat-Sen University, Kaohsiung 804, Taiwan

Supporting Information

ABSTRACT: A series of immiscible triple crystalline triblock copolymers, poly(ethylene oxide-*b*-ε-caprolactone-*b*-L-lactide) (PEO-*b*-PCL-*b*-PLLA), synthesized through sequential ring-opening polymerization, have been blended with phenolic resin. FTIR spectra revealed that the ether groups of the PEO blocks were stronger hydrogen bond acceptors for the OH groups of phenolic resin than were the C═O groups of the PCL and PLLA blocks. Curing of phenolic with the templates and hexamethylenetetramine resulted in excluded and confined PCL or PLLA phases, depending on the phenolic content. This effect led to the formation of various composition-dependent nanostructures, including disordered structures, bicontinuous gyroids, hexagonally packed cylinders, and spherical micelle structures. Small-angle X-ray scattering and transmission electron microscopy revealed that self-organized mesoporous phenolic resin formed at phenolic contents of only 30−50 wt % as a result of an intriguing balance among the contents of phenolic and the PEO, PCL, and PLLA blocks. An interesting closed-loop mesoporous structure existed in the phase diagram of the mesoporous phenolic resins templated by the PEO-*b*-PCL-*b*-PLLA triblock copolymers.

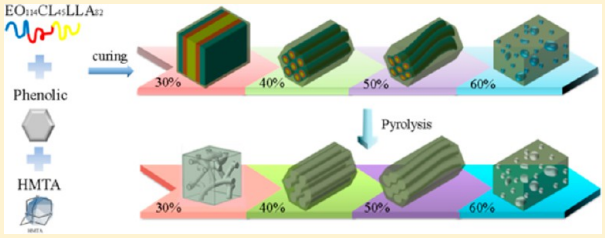

INTRODUCTION

Diblock copolymers can form many well-defined, self-assembled nanostructures in the bulk state, including spherical, hexagonally packed cylinder, gyroid, and lamellar structures.[1−4] Recently, there have been several investigations into the blending of homopolymers C with immiscible A-*b*-B diblock copolymers, where C can interact with the A or B block segments noncovalently (e.g., through hydrogen bonds).[5−21] For example, when C is miscible with B but immiscible with A,[5−8] we found that the ratio of the interassociation equilibrium constant (K_A) to the self-association equilibrium constant (K_B), K_A/K_B, is a convenient guide for estimating the phase behavior of A-*b*-B/C blends.[11] Very recently, Guo et al. and we reported another method to develop self-assembled nanostructures through competitive hydrogen bonding interactions.[11−20] In this second approach, C is both miscible with A and B blocks, but the hydrogen bonds between the B and C segments are stronger than those between the A and C segments. Hydrogen bonding interactions of different strengths lead to the formation of various composition-dependent microphase separations.[13,20]

The self-assembly of diblock copolymers in thermosets has been used to prepare ordered nanostructures.[22−25] Long-range-ordered nanostructures can form after mixing uncured phenolic resins with block copolymers featuring a block that interacts sufficiently strongly through hydrogen bonds with the phenolic OH groups, such that curing of the phenolic resin will preserve the self-assembled structure without it undergoing macroscopic phase separation.[26,27] In addition, ordered mesoporous phenolic resins having high surface areas and large pore volumes have received much attention for their potential applications in catalysis, photonics, adsorption, separation, and drug delivery.[28−30] For example, Ikkala et al. prepared mesoporous phenolic resins when using poly(isoprene-*b*-2-vinylpyridine) (PI-*b*-P2VP) and poly(styrene-*b*-4-vinylpyridine) (PS-*b*-P4VP) diblock copolymers as templates and hexamethylenetetramine (HMTA) as the curing agent.[7,8,31] Zheng et al. reported the formation of nanostructures in phenolic thermosets after curing novolac resins and the diblock copolymer poly(styrene-*b*-ethylene oxide) (PS-*b*-PEO) in the presence of HMTA. The use of novolac instead of resols resins can allow investigations of the morphological evolution before and after the curing reaction.[32] In all of studies mentioned above, the phenolic resin has been miscible with PEO, P2VP, and P4VP blocks as a result of hydrogen bonding, but immiscible with PI or PS blocks; thus, these systems can be classified as being examples of first case, where C is miscible with block B but immiscible with block A. In previous studies, we prepared poly(ethylene oxide-*b*-ε-caprolactone) (PEO-*b*-PCL) diblock copolymers, comprising two immiscible crystallizable blocks, PEO and PCL, that are both miscible with phenolic resin as a result of hydrogen bonding;[33−36] these systems have been A-*b*-B/C blends that are examples of the

Received: June 16, 2014
Revised: August 8, 2014
Published: September 10, 2014

dx.doi.org/10.1021/ma501246j | Macromolecules 2014, 47, 6389−6400

second case, where C is miscible with both A and B blocks. Because the hydrogen bonds formed between PEO blocks and phenolic resin are significantly stronger than those between PCL blocks and phenolic resin,[37,38] we have obtained various composition-dependent nanostructures from such systems, including distorted lamellae and gyroid structures.

In addition to the use of diblock copolymers, the self-assembly of hierarchical nanostructures from ABC triblock copolymers has been attractive because they can form three-phase lamellae, core/shell cylinders, and other hierarchical nanostructures in recent years.[1] Nevertheless, the self-assembly and morphological transitions that occur as a result of competitive hydrogen bonding in blends of a homopolymer D and an ABC triblock have rarely been investigated. To the best of our knowledge, only Guo et al. have reported the phase behavior of PS-*b*-P4VP-*b*-PEO/PVPh blends that results from competitive hydrogen bonding of the P4VP and PEO blocks with the polymer PVPh; they obtained a series of self-assembly nanostructures, including hexagonal cylinders, lamellae, disordered structures, and spherical microdomains, depending on the PVPh content.[39] In contrast, the use of ABC-type triblock copolymers as templates to prepare mesoporous materials has been reported widely.[40−46] For example, Zhao et al. prepared highly ordered mesoporous carbons having large mesopores and tunable mesopore walls after using the triblock copolymer PEO-*b*-PMMA-*b*-PS as a template and resol phenolic resin as a carbon source.[40] Vogt et al. obtained ordered mesoporous carbons when using poly(styrene-*b*- *N*,*N*,-dimethyl-*n*-octadecylamine-*b*-styrenesulfonate) (PS-*b*-DMODA-*b*-PSS)[41] and poly(ethylene oxide-*b*-ethyl acrylate-*b*-styrene) (PEO-*b*-PEA-*b*-PS)[42] as templates and resol phenolic resin as the carbon source. Yamauchi et al. described the synthesis of various mesoporous metal oxide materials of various compositions through the assembly of spherical polymeric micelles consisting of the triblock copolymer PS-*b*-P2VP-*b*-PEO.[43] Wiesner et al. prepared highly ordered mesoporous carbons after using PI-*b*-PS-*b*-PEO as a structure-directing triblock copolymer and resol phenolic resin as the carbon precursor. In each of those studies, the phenolic resin was miscible with only one or two of the blocks (e.g., PEO, P2VP, PMMA, or PEMA segments) as a result of intermolecular hydrogen bonding but was immiscible with the PS or PI segments. In addition, only the PEO block was crystalline in any of these triblock copolymer templates.

In this study, we investigated the behavior of PEO-*b*-PCL-*b*-PLLA triblock copolymers, comprising three immiscible crystallizable blocks, PEO, PCL, and PLLA, that are miscible with phenolic resin as a result of hydrogen bonding interactions. This system represents a new A-*b*-B-*b*-C/D blend type, where D is miscible with blocks A, B, and C. The strength of the hydrogen bonding interactions in this system follows the order phenolic/PEO > phenolic/PCL > phenolic/PLLA.[37,38,47] Several features have been observed in these blends: selective hydrogen bonding between the phenolic/PEO pair at relatively low phenolic contents; the coexistence of two competitive hydrogen bonding interactions (phenolic/PEO and phenolic/PCL pairs) at relatively high phenolic contents; and three competitive hydrogen bonding interactions (phenolic/PEO, phenolic/PCL, and phenolic/PLLA pairs) at the highest phenolic contents.[38] These effects led to the formation of various composition-dependent nanostructures, including disordered-sphere, cylinder, and gyroid structures. In this study, we used differential scanning calorimetry (DSC), Fourier transform infrared (FTIR) spectroscopy, small-angle X-ray scattering (SAXS), and transmission electron microscopy (TEM) to investigate the phase behavior of and competing interactions within these mesostructures. This paper describes the first examples of mesoporous phenolic resin prepared as a result of competitive hydrogen bonding in triple-crystalline triblock copolymer/homopolymer blends, where the homopolymer (phenolic) is miscible with all three of the block segments. We observed an interesting closed-loop[34,48−51] mesoporous structure in the phase diagram of the mesoporous phenolic resin templated by the PEO-*b*-PCL-*b*-PLLA triblock copolymers.

EXPERIMENTAL SECTION

Materials. Monomethoxypoly(ethylene glycol) with a molecular weight of 5000 (MPEG-5K) was obtained from Fluka and dried through azeotropic distillation with dry toluene. ε-Caprolactone (ε-CL, Acros) was purified through vacuum distillation over CaH_2; L-lactide was obtained from Alfa Aesar. Stannous(II) octoate [$Sn(Oct)_2$, Sigma] was used as received. CH_2Cl_2 was dried over CaH_2 prior to use. The phenolic was synthesized through condensation with H_2SO_4 with an average molecular weight (M_n) of 500, as described previously.[52−54] Hexane, tetrahydrofuran (THF), and HMTA were used as received. Deionized water was used in all experiments.

Synthesis of PEO-*b*-PCL-*b*-PLLA Triblock Copolymers. Triblock copolymers were prepared through ring-opening polymerization (ROP) of L-lactide with the diblock copolymer PEO-*b*-PCL (which had also been synthesized through ROP) as the macroinitiator and $Sn(Oct)_2$ as the catalyst.[55] The diblock copolymer PEO_{114}-*b*-PCL_{45} was prepared through ROP of ε-CL and mPEG-5K in the presence of $Sn(Oct)_2$.[33,56] The reaction mixtures were prepared by introducing a desired volume of ε-CL monomer into a silanized flask containing a preweighed amount of mPEG-5K under a N_2 atmosphere. $Sn(Oct)_2$ was added, and then the flask was connected to a vacuum line, evacuated, sealed off, and heated at 130 °C. After 24 h, the resulting block copolymers were dissolved in CH_2Cl_2 and precipitated in an excess of cold *n*-hexane. The triblock copolymers PEO-*b*-PCL-*b*-PPLA were prepared by placing a desired weight of L-lactide in a silanized flask containing a preweighed amount of PEO-*b*-PCL under a N_2 atmosphere. $Sn(Oct)_2$ (several drops) was added, and then the flask was connected to a vacuum line, evacuated, sealed off, and heated at 130 °C. After 24 h, the resulting block copolymers were dissolved in CH_2Cl_2 and precipitated in an excess of cold *n*-hexane. The triblock copolymers were dried at 40 °C under vacuum; their characterization data are listed in Table 1.

Table 1. Characterization of PEO-*b*-PCL-*b*-PLLA Triblock Copolymers Used in This Study

sample	abbrev	M_n (^{1}H NMR)	M_n (GPC)	M_w (GPC)	PDI
$EO_{114}CL_{45}LLA_{19}$	ECL1	11 514	24 900	27 480	1.10
$EO_{114}CL_{45}LLA_{57}$	ECL2	13 908	25 030	28 540	1.14
$EO_{114}CL_{45}LLA_{82}$	ECL3	16 050	25 190	29 470	1.17
$EO_{114}CL_{45}LLA_{108}$	ECL4	17 922	30 520	36 620	1.20

Synthesis of Mesoporous Phenolic Resins. Phenolic resin, HMTA, and PEO-*b*-PCL-*b*-PLLA were dissolved in THF until the solutions were homogeneous. The solvent was evaporated slowly at room temperature, and then the residue was vacuum-dried at 50 °C for 24 h. Curing of the samples was performed using the following temperature profiles: 100 °C for 2 h, 150 °C for 2 h, and 190 °C for 0.5 h. Pyrolysis of the cross-linked phenolic samples was performed by slowly heating from room temperature to 330 °C at a heating rate of 1 °C min^{-1} in the absence of a protective gas atmosphere.

Characterization. ^{1}H NMR spectra were recorded at room temperature using a Bruker AM 500 (500 MHz) spectrometer, with residual proton resonance of the deuterated solvent ($CDCl_3$) as the

dx.doi.org/10.1021/ma501246j | Macromolecules 2014, 47, 6389−6400

internal standard. Molecular weights and molecular weight distributions were determined through gel permeation chromatography (GPC) using a Waters 510 HPLC equipped with a 410 differential refractometer and three Ultrastyragel columns connected in series; DMF was the eluent at a flow rate of 1.0 mL min^{-1}. Thermal analysis was performed through differential scanning calorimetry (DSC) using a Q-20 differential scanning calorimeter; the instrument was operated at a heating rate of 20 °C min^{-1} and a cooling rate of 5 °C from 180 to −90 °C under N_2. FTIR spectra of the samples were recorded using the conventional KBr disk method and a Bruker Tensor 27 FTIR spectrophotometer. SAXS experiments were performed using the SWAXS instrument at the BL17B3 beamline of the NSRRC, Taiwan; the X-ray beam had a diameter of 0.5 mm and a wavelength (λ) of 1.24 Å. In-situ SAXS measurements were performed using a Nanostar U small-angle X-ray scattering system (Bruker, Germany) and Cu Kα radiation (40 kV, 35 mA). Nitrogen sorption isotherms were measured at 77 K using an ASAP 2020 analyzer. Prior to measurement, the samples were degassed under vacuum at 200 °C for at least 6 h. The pore volumes and pore size distributions were derived from the adsorption branches of the isotherms; the total pore volumes were estimated from the adsorbed amount at a relative pressure (P/P_0) of 0.995. The calibration curve was obtained using silica−alumina (part no. 004-16821-00) as the reference material and N_2 as the adsorption gas. TEM experiments were conducted using a JEOL 3010 microscope (Japan) operated at 200 kV.

RESULTS AND DISCUSSION

Analyses of Triblock Copolymers. A PEO-*b*-PCL diblock copolymer having a high molecular weight (ca. 10 130 g mol^{-1}) was readily prepared through a simple one-step ROP.[55] We determined the number-average molecular weight (M_n) of our prepared diblock copolymer from its ^1H NMR spectrum, comparing the peak intensity of the signal for the ethylene units (CH_2CH_2O) of MPEG-5K (δ = 3.65 ppm) with that of the methylene units (OCH_2) of PCL (δ = 4.10 ppm) in Figure 1b,

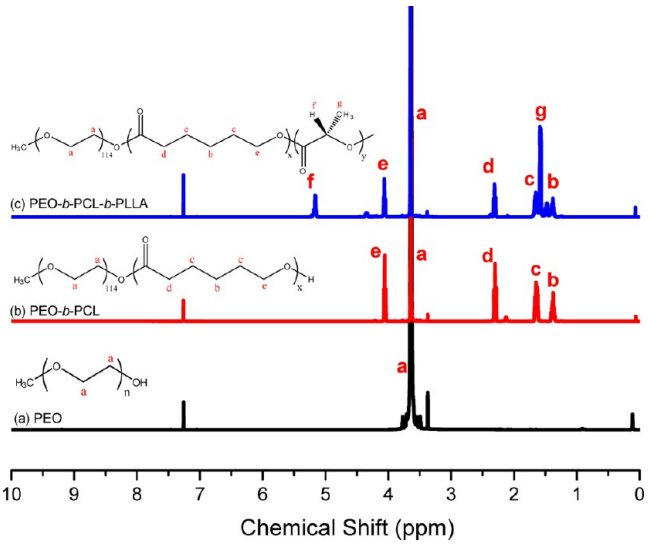

Figure 1. ^1H NMR spectra of (a) pure PEO, (b) the diblock copolymer PEO-*b*-PCL, and (c) the triblock copolymers PEO-*b*-PCL-*b*-PLLA.

considering the molecular weight (M_n = 5000) of MPEG-5K (Figure 1a). To study the phase behavior of various mesoporous phenolic samples templated by ABC triblock copolymers PEO-*b*-PCL-*b*-PLLA, we prepared four different PEO-*b*-PCL-*b*-PLLA templates of high molecular weight through simple ROP using our PEO−PCL diblock copolymer ($EO_{114}CL_{45}$; M_n = 10 130 g mol^{-1}) as the macroinitiator, $Sn(Oct)_2$ as the catalyst, and THF as the solvent. GPC revealed a narrow polydispersity index (PDI, Figure 2, Table 1) for each

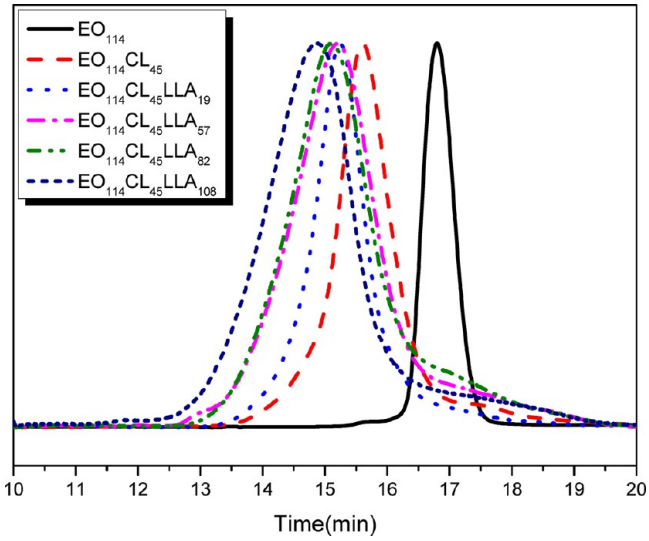

Figure 2. GPC traces of pure PEO, the diblock copolymer PEO-*b*-PCL, and the triblock copolymers PEO-*b*-PCL-*b*-PLLA.

triblock copolymer; we determined values of M_n from their ^1H NMR spectra (Figure 1c), comparing the peak intensities of their protons $\mathbf{H}_f$ (δ = 5.17 ppm) with those of PEO-*b*-PCL-*b*-PLLA (Table 1). We performed SAXS analyses to determine the self-assembled structure formed using our four PEO-*b*-PCL-*b*-PLLA templates (Figure S1). Table 1 lists the specific compositions of our PEO-*b*-PCL-*b*-PLLA triblock copolymers.

Thermal Analyses. We have reported that PVPh, phenolic, and bisphenol A (BPA) are totally miscible with PEO, PCL, and PLLA in the amorphous phase as a result of interassociation hydrogen bonding between the OH groups of the phenolic resins and either the C═O groups of PCL and PLLA or the ether groups of PEO.[37,38,47] In general, DSC is a convenient method for determining the miscibility of polymer blends. The glass-transition temperatures (T_g) of the pure polymers used in this study—phenolic, PEO, PCL, and PLLA—are 66, −60, −60, and 57 °C, respectively.[37,47] Figure 3 displays the conventional second-run DSC thermograms of various compositions of phenolic/ECL (here, ECL represents PEO-*b*-PCL-*b*-PLLA) blends (not cured with HMTA), recorded at a heating rate of 20 °C min^{-1}. The melting temperatures of the PEO, PCL, and PLLA blocks were all depressed, ultimately disappearing completely, upon increasing the content of phenolic resin in all four of our blend systems. The decreases in the melting temperatures resulted from morphological effects and the thermodynamic consequences of hydrogen bonding with the phenolic resins.[47,57−60] Table 2 summarizes the thermal properties of our phenolic/ECL blends, determined through DSC analyses.

Thermal analyses of these phenolic/ECL blends are complicated because the values of T_m of PEO and PCL are very similar and also very close to those of PPLA and phenolic resin (ca. 50−65 °C). Fortunately, the interassociation equilibrium constants between the phenolic OH groups and the ether groups of PEO (K_A = 264), the C═O groups of PCL (K_A = 116), and the C═O groups of PLLA (K_A = 10) are all different, such that the formation of hydrogen bonds between

dx.doi.org/10.1021/ma501246j | Macromolecules 2014, 47, 6389−6400

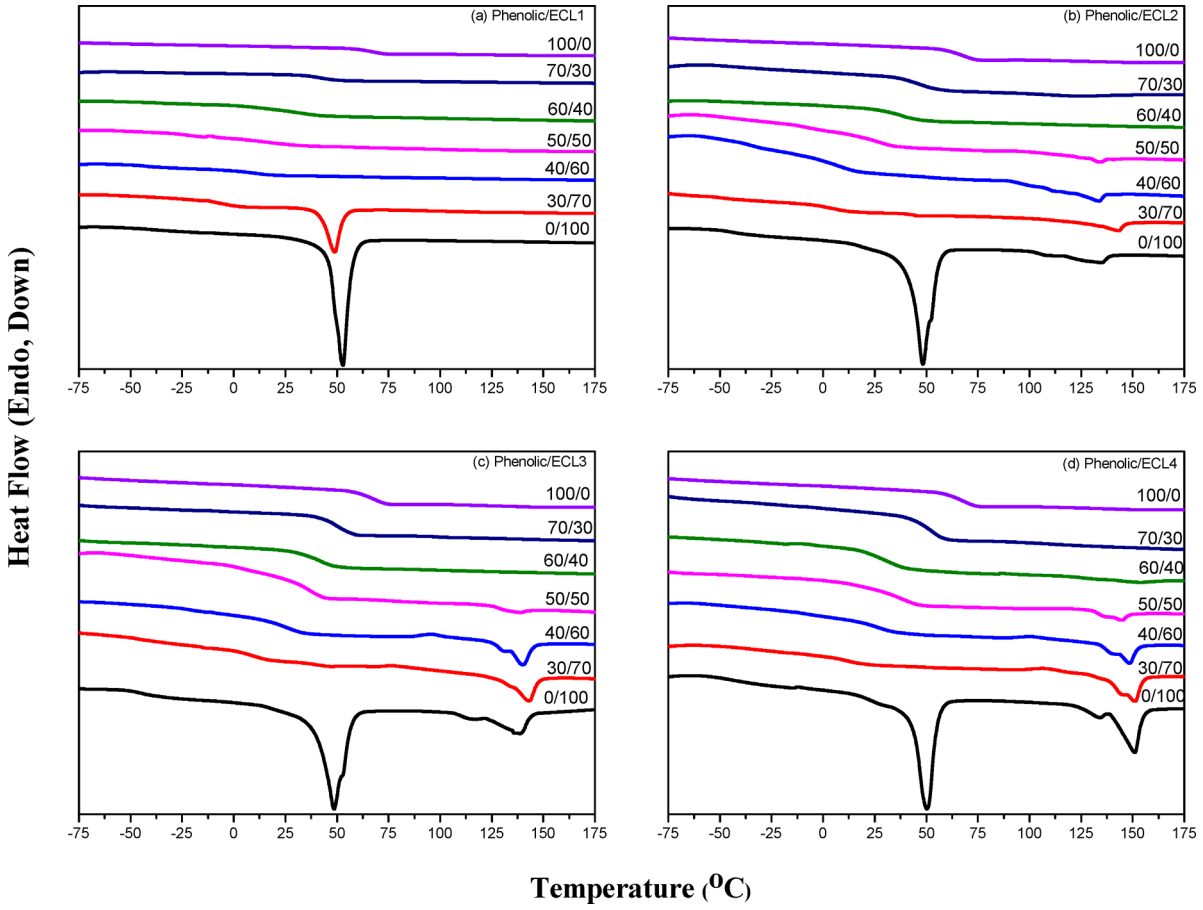

Figure 3. DSC thermograms of phenolic/ECL blends of various compositions: (a) phenolic/ECL1, (b) phenolic/ECL2, (c) phenolic/ECL3, and (d) phenolic/ECL4.

phenolic and the PEO blocks predominates over those between phenolic and the PCL or PLLA blocks in these phenolic/ECL blends.[37,38] For the pure ECL triblock copolymers, we observed a value of T_g of approximately −45 °C and a value of T_m of approximately 50 °C, presumably representing both the PEO and PCL block segments, and a value of T_m of approximately 135−150 °C that was strongly dependent on, and presumably representing, the molecular weight of the PLLA blocks. We did not observe glass transition behavior of the PLLA blocks because it is overlapped with the melting of the PEO and PCL blocks.

After blending with 30−50 wt % of phenolic resin, the melting peaks (ca. 50 °C) for the PEO and PCL blocks disappeared, but the melting peaks (ca. 135−150 °C) for the PLLA blocks of the triblock copolymers ECL2, ECL3, and ECL4 remained. This behavior is reasonable because the values of K_A followed the order phenolic/PEO > phenolic/PCL > phenolic/PLLA; therefore, most of the OH groups of phenolic interacted with the ether groups of PEO blocks and the C═O groups of the PCL blocks at relatively low phenolic contents (30−50 wt %) but did not interact with the C═O groups of the PLLA blocks. Further increases in the phenolic content (to 60−70 wt %) caused the melting peaks of the PLLA blocks to also disappear, implying that the OH groups of phenolic were also able to interact with the C═O groups of the PLLA blocks under these conditions and, thus, induced the miscible behavior at these relatively high phenolic contents. The two values of T_g of the PEO and PCL blocks shifted higher in the presence of 30−50 wt % of the phenolic resin. The changes in the values of T_g arose from the phenolic−PEO (higher T_g) and the phenolic−PCL (lower T_g) phases because the interassociation equilibrium constant for the interactions of the phenolic OH groups with the ether groups of the PEO blocks was greater than the interassociation equilibrium constant for the interactions of the OH groups of phenolic with the C═O groups of the PCL blocks.[37] The phenolic/ECL blends exhibited only one glass transition temperature when the phenolic content was greater than 60 wt %, suggesting that these blends had become miscible. Figure 4 reveals that the experimental values of T_g were larger than those calculated from the linear prediction, consistent with strong hydrogen bonding within our phenolic/ECL blends.[38]

FTIR Spectroscopic Analyses. As mentioned in our discussion of the DSC results, the strength of the hydrogen bonds in a phenolic/PEO system is greater than those in phenolic/PCL and phenolic/PLLA blend systems. When the phenolic content is sufficiently high, its OH groups become available for interaction with all of the PEO, PCL, and PLLA blocks through hydrogen bonding. At 60 wt % phenolic, the blends became miscible, with phenolic acting as a common solvent in these blend systems. We used FTIR spectroscopy to provide evidence of this common solvent effect. Several regions within the FTIR spectra of the phenolic/ECL blends were influenced by the hydrogen bonding interactions. For convenience, selected FTIR spectra of only the phenolic/ECL3 blends are presented herein. Figure 5 presents the OH

dx.doi.org/10.1021/ma501246j | Macromolecules 2014, 47, 6389−6400

Table 2. Thermal Properties of Phenolic/ECL Blends

phenolic/ECL	T_g (°C)	T_m (°C)	ΔH_f (J/g)
pure phenolic	66		
phenolic/ECL1			
70/30	42.5		
60/40	32.2		
50/50	−21.8 14.5		
40/60	−43.5 10.7		
30/70	−6.9	49.0	22.5
0/100	–	53.0	83.5
phenolic/ECL2			
70/30	49.6		
60/40	38.4		
50/50	−12 25.5	134.6	0.7
40/60	−36.3 5.9	134.0	1.6
30/70	−50.4 2.7	143.5	3.6
0/100	−45.6	48.4 135	49.2 4.0
phenolic/ECL3			
70/30	52.3		
60/40	42		
50/50	−10.2 35.9	139.2	0.8
40/60	−21.8 24.6	140.0	5.4
30/70	−48 10.5	143.0	7.7
0/100	−46	48.7 140	33.7 12.4
phenolic/ECL4			
70/30	52.6		
60/40	43.0		
50/50	−1.2/36.5	145.2	1.4
40/60	−19.9 25.5	148.4	5.8
30/70	−30.9 12.4	152.0	10.1
0/100	−46.9	50.3 153.0	30.9 10.5

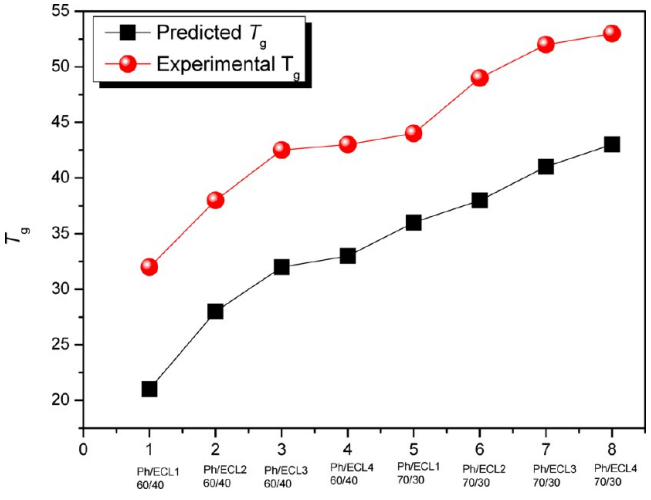

Figure 4. Glass transition temperatures from predicted and experimental data.

stretching bands of various phenolic/ECL3 blends and those of pure phenolic cast from THF solution. The spectrum of pure phenolic (Figure 5a) features two unresolved bands in the OH stretching region: one corresponding to the free OH groups at 3525 cm^{-1} and the other broad band centered at 3350 cm^{-1} corresponding to the absorption of hydrogen-bonded OH groups (self-association). The intensity of the band for the free OH groups gradually decreased upon increasing the ECL3 content in this blend system, as would be expected. From the Painter−Coleman association model,[61,62] the interassociation

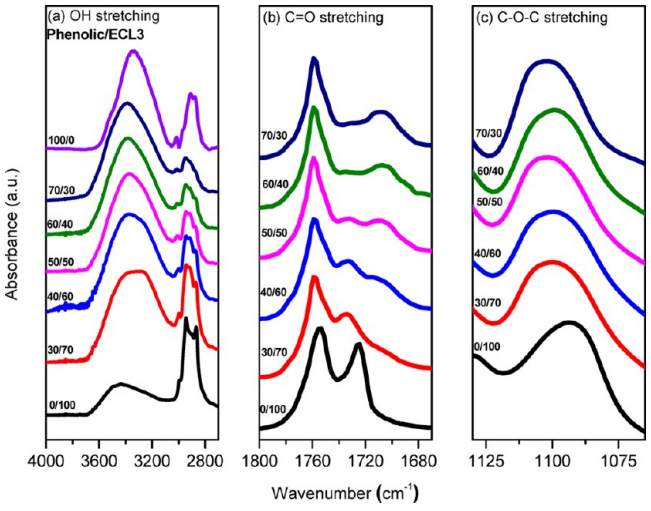

Figure 5. FTIR spectra recorded at room temperature of phenolic/ECL3 blends: (a) OH stretching, (b) C═O, and (c) ether regions.

equilibrium constant of the phenolic/PEO blend (K_A = 264) is greater than those of phenolic/PCL (K_A = 116) and phenolic/PLLA (K_A = 10) blends, implying that the formation of hydrogen bonds between phenolic and the PEO blocks predominates over those between phenolic and the PCL or PLLA blocks in these phenolic/ECL blends.[38] As a result, the OH band shifted to lower wavenumber when the blend contained a low phenolic content (30 wt %), implying that the phenolic OH groups interacted preferably with the ether units of the PEO blocks. Therefore, it is reasonable to assign the band at 3275 cm^{-1} to the OH groups that were hydrogen bonded to the ether units because the OH groups of a relatively low content of phenolic tended to interact completely, through hydrogen bonds, with the ether groups of the PEO blocks. The peak frequency of the broad band shifted to higher wavenumber upon increasing the phenolic content (>70 wt %). This shift reflects a new distribution of the hydrogen bonds resulting from competition among the OH···OH interactions within the pure phenolic and the OH···O═C interactions between phenolic and the PCL or PLLA blocks (3385 cm^{-1}).

Figure 5b reveals that the signals for the C═O groups of the PCL and PLLA blocks were sensitive to the presence of hydrogen-bonding interactions. The bands at 1724 and 1753 cm^{-1} correspond to the crystalline conformations of the C═O groups of the PCL and PLLA blocks, respectively. Increasing the phenolic content caused the crystalline conformations of these peaks to disappear, with the signals moving to 1734 and 1758 cm^{-1}, representing the amorphous conformations of the PCL and PLLA blocks, respectively.[37,47] This finding is consistent with our DSC analyses, in which the melting peaks disappeared upon increasing the phenolic contents. In addition, we found that the band for the hydrogen-bonded C═O groups of the PCL block at 1705 cm^{-1} began to appear in the blends when the phenolic content was 30 wt % or greater, suggesting that the phenolic OH groups began to interact with the C═O groups of the PCL blocks. As expected, a higher content of phenolic resulted in a higher number of hydrogen-bonded C═O groups. In contrast, the hydrogen bonds between phenolic and the PLLA blocks were not strong: we observed no significant shift in the wavenumber of the C═O groups for the PLLA blocks, consistent with the behavior of PVPh/PLLA and BPA/PLLA blends.[47,63] As a result, we in this study could

dx.doi.org/10.1021/ma501246j | Macromolecules 2014, 47, 6389−6400

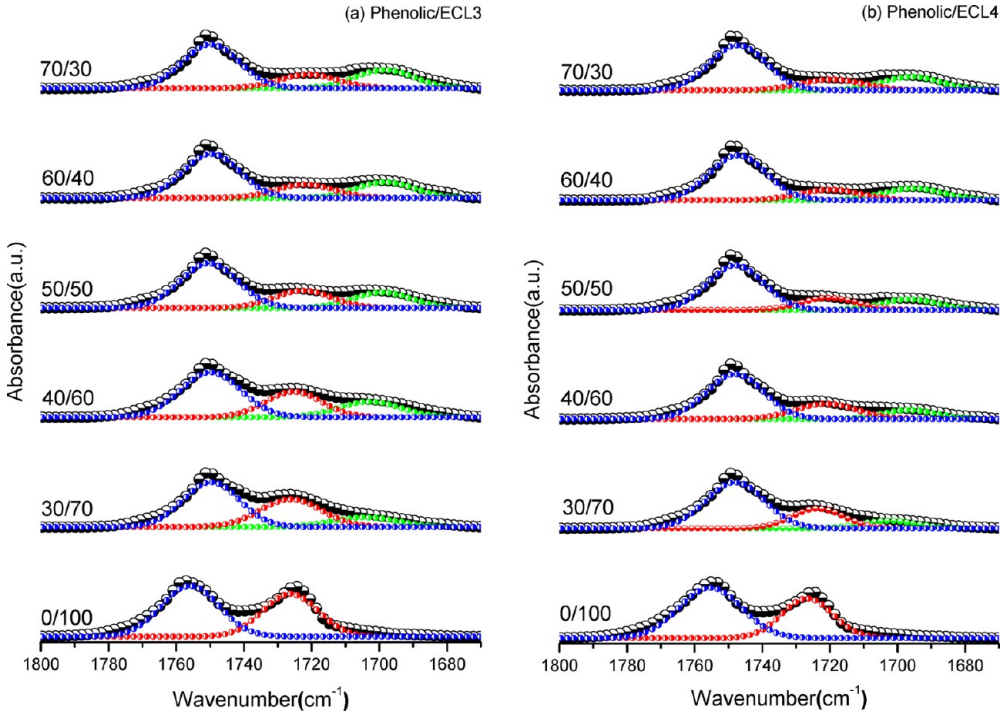

Figure 6. Data from curve fitting of the FTIR spectra of (a) phenolic/ECL3 and (b) phenolic/ECL4 blends.

Table 3. Curve Fitting Results of Phenolic/ECL Blends

	free C═O for LLA		free C═O for CL		HBC═O for CL		
	ν (cm^{-1})	A_a (%)	ν (cm^{-1})	A_b (%)	ν (cm^{-1})	A_c (%)	f_b (%)
phenolic/ECL1							
0/100	1756.0	26.1	1727.2	73.9			
30/70	1760.0	24.6	1733.5	75.4			
40/60	1759.4	19.7	1733.0	61.8	1708.1	18.5	16.63
50/50	1758.4	22.3	1732.9	42.8	1708.6	34.9	35.21
60/40	1756.9	19.6	1731.9	36.6	1707.3	43.7	44.32
70/30	1756.5	21.0	1731.6	29.1	1708.0	50.0	53.39
phenolic/ECL2							
0/100	1757.6	60.0	1731.5	40.0			
30/70	1756.7	45.8	1733.4	37.7	1711.1	16.4	22.48
40/60	1757.6	40.5	1733.4	38.4	1709.9	21.0	26.71
50/50	1757.2	40.8	1732.9	29.8	1708.4	29.4	39.67
60/40	1756.5	40.3	1732.0	27.3	1707.3	32.4	44.17
70/30	1756.8	36.4	1733.7	27.6	1706.6	36.0	46.51
phenolic/ECL3							
0/100	1756.0	55.4	1726.3	44.6			
30/70	1749.7	52.2	1726.2	35	1704.3	12.8	19.60
40/60	1749.9	53.0	1725.4	28.2	1702.9	18.8	30.76
50/50	1750.4	57.5	1722.7	22.4	1699.3	20.1	37.43
60/40	1749.7	59.2	1722.0	18.7	1698.3	22.1	44.06
70/30	1749.9	56.9	1721.0	18.5	1698.6	24.6	46.99
phenolic/ECL4							
0/100	1755.4	61.0	1726.7	39.0			0
30/70	1748.1	65.3	1723.6	24.6	1702.8	10.2	21.65
40/60	1748.1	64.7	1721.6	23.3	1696.5	18.5	34.61
50/50	1748.0	66.1	1720.2	18.0	1696.5	19.5	41.93
60/40	1747.3	65.4	1719.9	16.2	1695.4	18.4	43.09
70/30	1747.3	63.3	1719.4	16.9	1696.0	19.7	43.72

ignore the hydrogen bonding of the C═O groups for the PLLA blocks for curve fitting. Figure 6 summarizes the results obtained from curve-fitting (Gaussian function) for these three bands in the phenolic/ECL3 and phenolic/ECL4 blends. We could calculate the fraction of hydrogen-bonded C═O groups using an absorptivities ratio ($a = a_{HB}/a_F = 1.5$) in accord with

dx.doi.org/10.1021/ma501246j | Macromolecules 2014, 47, 6389−6400

previous studies of the FTIR spectra of systems undergoing OH···O=C interassociation.[38] Table 3 summarizes the results from curve fitting of all of our phenolic/ECL blends; it indicates that the fraction of hydrogen-bonded C=O groups increased upon increasing the phenolic content.

We could also use the band at 1100 cm^{-1} to analyze the hydrogen bonding between the OH groups of phenolic and the ether units of the PEO blocks. Figure 5c displays scale-expanded (1050−1140 cm^{-1}) FTIR spectra for the phenolic/ECL3 blends. The spectrum of pure ECL3 featured a characteristic band at 1092 cm^{-1} that corresponded to the C−O−C absorptions of the PEO block. Upon the formation of hydrogen bonds between phenolic and the PEO block, this band shifted to 1100 cm^{-1}, consistent with hydrogen-bonded ether units at phenolic resin contents of 30 wt % or greater.[64]

Reaction-Induced Microphase Separation of Cured Phenolic/ECL Blends. We investigated the thermal behavior of phenolic/ECL blends prepared in the presence of HMTA as a curing agent. Although microphase separation existed in the cured blends of phenolic thermosets with the blocks, it could have resulted from reaction-induced demixing from homogeneous mixtures.[65] Figure S2 displays the DSC traces (second run heating scans) of phenolic/ECL3 blends cured with HMTA. Two melting peaks appeared for the phenolic/ECL3 = 30/70 blends that were different from that of the same system in the absence of HMTA curing. The peak at the lower melting temperature may have arisen from the PEO or PCL block segments through a reaction-induced microphase separation mechanism. Thermal curing can inhibit intermolecular hydrogen bonding between the OH groups of phenolic and the ether units of PEO blocks or the C=O groups of PCL blocks, such that curing can affect the morphologies of phenolic/PEO and phenolic/PCL blends remarkably.[65,66] To understand the subsequent curing steps of these complicated mixtures, especially through in-situ observation of the curing process,[36] we used in-situ SAXS during various curing periods to obtain kinetic SAXS data (Figure 7). These kinetic SAXS measurements reveal extremely different behavior that can be distinguished within two different periods. In the first, from 40 to 100 °C, the SAXS patterns reveal a transformation from disorder to short-range order (single peak); in the second, between 100 and 150 °C, we observed an interesting feature: the single broad scattering peak tended toward a sharp peak and a weaker peak at a ratio of 1:2:3, suggesting the development of representative lamellar packing. Clearly, the regularity of cross-linked samples was enhanced through a reaction-induced microphase separation mechanism, which is consistent with in-situ FTIR spectra analysis (Figure S3) that the hydrogen-bonded carbonyl group of PCL was decreased with the increase of thermal curing temperature.

Next, we recorded SAXS profiles of the phenolic/ECL3 blends after curing to confirm the self-organized morphologies (Figure 8). The pure ECL3 block copolymer exhibited short-range order of lamellar character, as determined by the special ratio of q^* and $2q^*$, consistent with the TEM image in Figure 9a. At a phenolic content of 30 wt %, we observed long-range order at q/q_{max} ratios of 1, 2, 3, and 4, corresponding to the long-range order of a lamellar structure, which also be observed in the TEM image in Figure 9b. We also observed, however, some local long-range order of gyroid structures, as revealed in the TEM images in Figures 9c,d, at phenolic content of 30 wt %. From SAXS analyses, we also observed signals at a $\sqrt{6}:\sqrt{8}$ ratio, corresponding to a bicontinuous packing (gyroid)

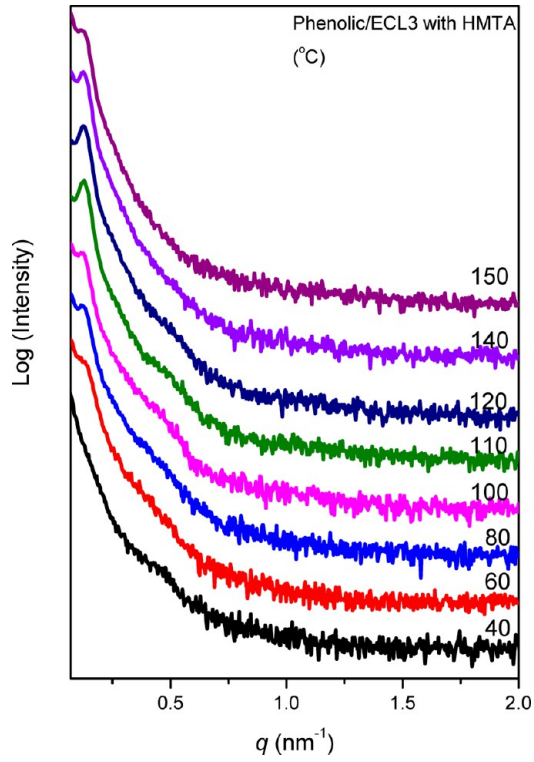

Figure 7. In-situ SAXS patterns recorded during the curing reaction of the phenolic/ECL3 blend in the presence of HMTA.

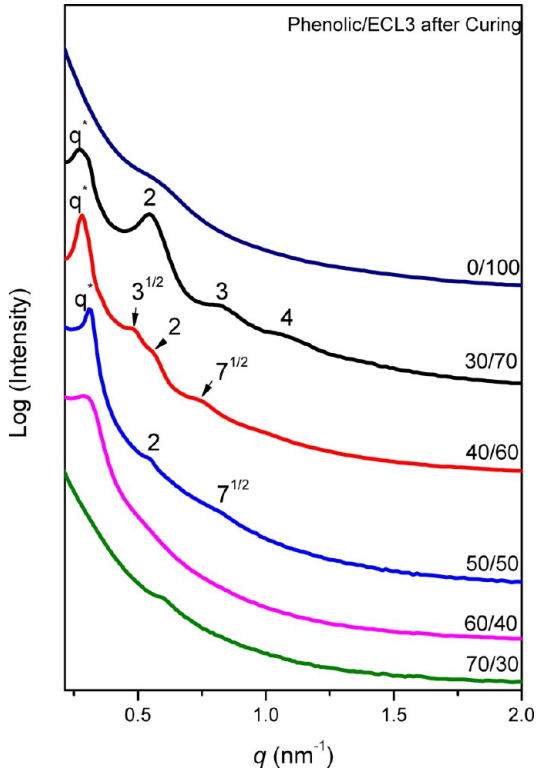

Figure 8. SAXS patterns of phenolic/ECL3 blends after curing in the presence of HMTA.

structure. Increasing the phenolic content to 40 wt %, the single scattering peak tended toward a set of specific peaks in a ratio of $1:\sqrt{3}:\sqrt{4}:\sqrt{7}$, indicating the development of representative hexagonal cylindrical packing, as confirmed in

dx.doi.org/10.1021/ma501246j | Macromolecules 2014, 47, 6389−6400

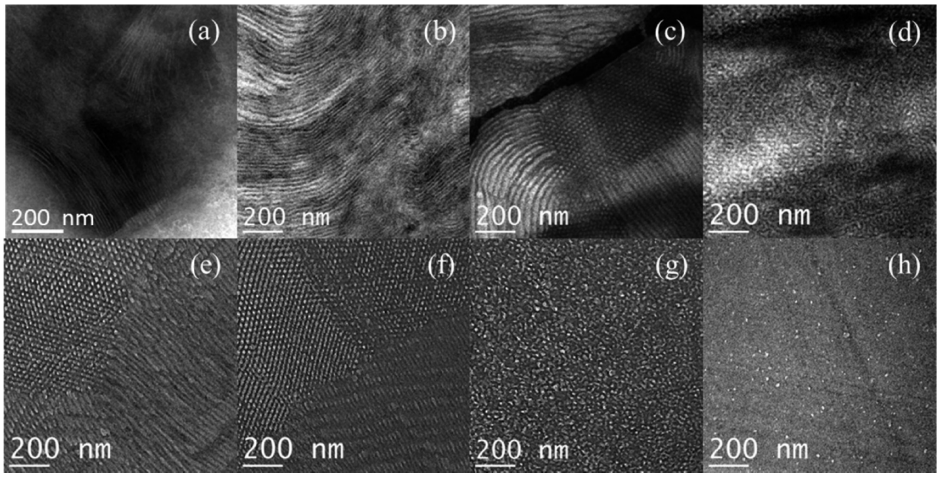

Figure 9. TEM images of phenolic/ECL3 blends after curing in the presence of HMTA: (a) pure ECL3, (b–d) 30/70, (e) 40/60, (f) 50/50, (g) 60/40, and (h) 70/30.

the TEM image in Figure 9e. Further increasing the phenolic content to 50 wt % resulted in the absence of a long-range ordered structure, with a small peak near $\sqrt{7}$ arising from incomplete disordering of the hexagonal cylinders, again confirmed in the TEM image in Figure 9f. The SAXS profiles revealed only weak and broad peaks at phenolic contents of greater than 60 wt %, suggesting near-disordered and short/long-ordered morphologies. These are characteristic of a disordered spherical and miscible structure, which we confirmed through the TEM images in Figures 9g,h. The blends containing 60 and 70 wt % phenolic were miscible, with phenolic acting as a common solvent as a result of its hydrogen bonding with all of the PEO, PCL, and PLLA block segments, based on DSC and FTIR spectroscopic analyses. In addition, according to the positions of the first-order scattering peaks for the samples containing 30, 40, and 50 wt % phenolic, the average spacings between the neighboring microdomains were 23.6, 22.5, and 20.4 nm, respectively, indicating that the size of the microphase domains decreased systemically upon increasing the phenolic content. We observed similar trends in the SAXS analyses of our phenolic/ECL1 and phenolic/ECL4 blends after curing (Figures S4a and S4b, respectively).

SAXS, TEM, and BET Analyses of Mesoporous Phenolic Resins. After performing the curing processes, we used calcination to remove the ECL templates and construct mesoporous phenolic resins. In-situ SAXS performed during the calcination process (Figure 10), and we also compare the SAXS patterns obtained before curing and after curing and the calcination system after this particular process as shown in Figure S5. The results revealed that the higher-order reflection peak become sharper upon removal of the ECL3 template, leading to pore formation and greater contrast in electron density. In addition, the first peak shifted to a lower value of q upon increasing the temperature due to the thermal expansion. We observed the lamellar structure, with q/q_{max} ratios of 1 and 2, for the phenolic/ECL3 = 30/70 blend after curing at room temperature. The SAXS profile of the final pyrolyzed product displayed a characteristic $\sqrt{6}$:$\sqrt{8}$ reflection ratio, confirming that a gyroidal structure remained after calcination. The primary SAXS scattering was located at 0.27 nm^{-1}. This value of $\sqrt{6}q^*$ indicated the reflection viewed from [211]; we calculated a d-spacing of 23.2 nm and used the equation $a = 6^{1/2}d_{211}$ to determine a value for the cell parameter a of 56.8

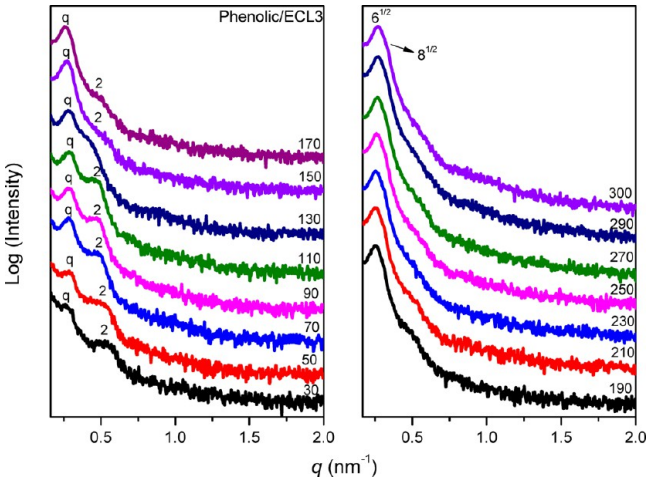

Figure 10. In-situ SAXS patterns recorded during the calcination of the cured phenolic/ECL3 = 30/70 blend.

nm. Figure 11 summarizes all of the SAXS profiles of our mesoporous phenolic resins templated by the ECL triblock copolymers recorded at room temperature to confirm the self-organized mesoporous morphologies.

Figure 11a displays the SAXS profile of a mesoporous phenolic resin templated by ECL1 triblock copolymer; we observe broad peaks corresponding to short-range-ordered mesoporous phenolic resin at relatively lower phenolic contents (30 wt %), consistent with the TEM image in Figure 12a. The profiles of the blends containing 40 and 50 wt % phenolic featured a sharp first peak and a shoulder peak with $\sqrt{3}$, corresponding to a cylindrical mesoporous structure, as confirmed through the TEM images in Figures 12b and 12c, respectively. Only broad peaks appeared in the SAXS pattern recorded at a phenolic content of 60 wt %, indicating a near-disordered and short/long-ordered morphology, as revealed in the TEM image in Figure 12d. The blends containing 70 wt % phenolic were miscible, with the phenolic acting as a common solvent, with a disordered structure in the TEM image (Figure 12e). Figure 11b displays the SAXS profiles of the mesoporous phenolic resin templated by the ECL2 triblock copolymer; we observe very similar mesophase transformations upon increasing the content of phenolic resin, from short-range order (at 30

dx.doi.org/10.1021/ma501246j | Macromolecules 2014, 47, 6389–6400

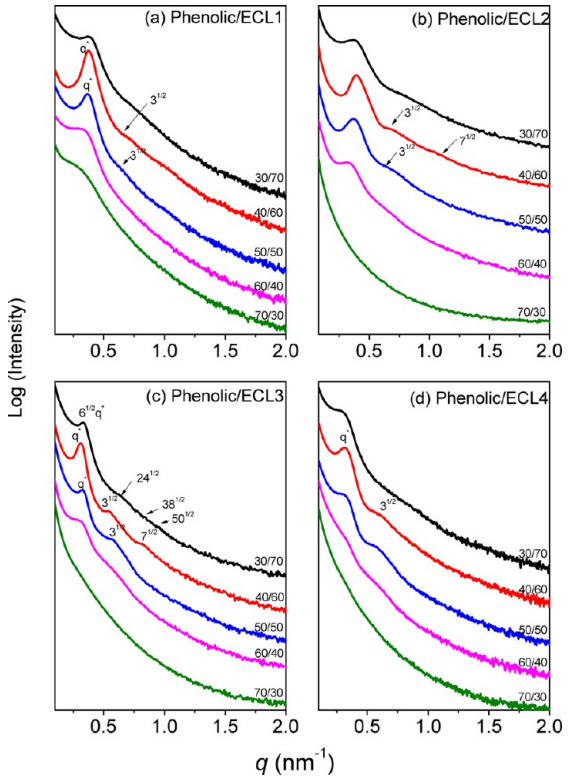

Figure 11. SAXS patterns of mesoporous phenolic resins templated by the triblock copolymers (a) ECL1, (b) ECL2, (c) ECL3, and (d) ECL4.

wt % phenolic; TEM image in Figure 12f), to cylindrical structures (40−50 wt %; TEM images in Figures 12g,h; Figure S6 displays microtome images of the sample in Figure 12g), to a near-disordered and short/long-ordered structure (60 wt %; TEM image in Figure 12i), and finally to a disordered structure (70 wt %; TEM image in Figure 12j). This behavior was very similar to that of the mesoporous phenolic templated by the triblock copolymer ECL1. Figure 11c presents the SAXS profiles of the mesoporous phenolic resins templated by the triblock copolymer ECL3; upon increasing the content of phenolic resin, we observed a remarkable mesophase transformation from a bicontinuous gyroid structure (30 wt %), to cylindrical structures (40−50 wt %), to short cylinders (60 wt %), and finally to a disordered structure (70 wt %). For the ordered bicontinuous gyroid structure observed at 30 wt % phenolic, the intensity maxima in the SAXS profile appeared at $\sqrt{6}q^*$, $\sqrt{24}q^*$, $\sqrt{38}q^*$, and $\sqrt{50}q^*$ (inset to Figure 11c), characteristic with the long-range order in a bicontinuous gyroid structure. The TEM image in Figure 12k confirmed this structure. For the blends containing phenolic contents of 40 and 50 wt %, the maximum intensities appeared at approximately q^* with higher-order reflections at $\sqrt{3}:\sqrt{4}:\sqrt{7}$; these values are characteristic of a long-range-ordered cylindrical structure, which we further confirmed through the TEM images in Figures 12l and 12m, respectively. At 60 wt % phenolic, however, the SAXS profile suggested a short-range-ordered spherical structure, based on the appearance of broad peaks that indicated the absence of a long-range-ordered structure; again, TEM confirmed this behavior (Figure 12n). A disordered structure without any SAXS peaks appeared at a phenolic content of 70 wt % (confirmed by the TEM image in Figure 12o). Scheme 1 summarizes the possible mesophase

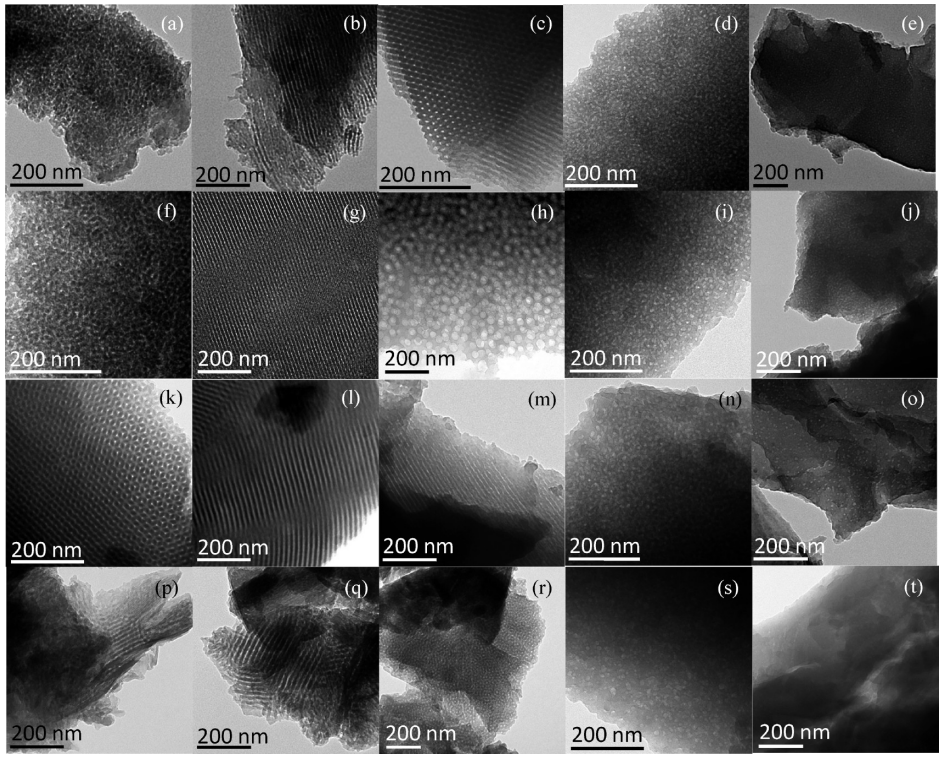

Figure 12. TEM images of mesoporous phenolic structures obtained from phenolic/ECL1 blends: (a) 30/70, (b) 40/60, (c) 50/50, (d) 60/40, and (e) 70/70; phenolic/ECL2 blends: (f) 30/70, (g) 40/60, (h) 50/50, (i) 60/40, and (j) 70/30; phenolic/ECL3 blends: (k) 30/70, (l) 40/60, (m) 50/50, (n) 60/40, and (o) 70/70; and phenolic/ECL4 blends: (p) 30/70, (q) 40/60, (r) 50/50, (s) 60/40, and (t) 70/30.

dx.doi.org/10.1021/ma501246j | *Macromolecules* 2014, 47, 6389−6400

Scheme 1. Morphological Changes in Self-Assembled Nanostructures and Mesoporous Phenolic Resins Templated by the Triblock Copolymer ECL3

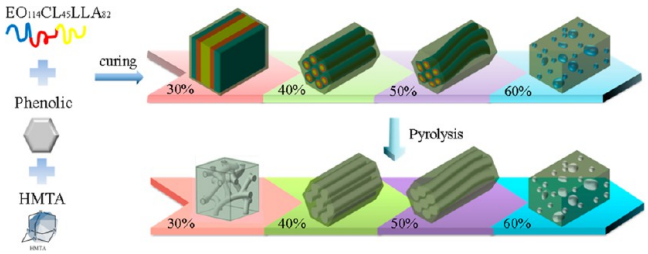

transitions that occurred upon increasing the phenolic content when templated by the triblock copolymer ECL3. Similarly, Figure 11d displays the SAXS profiles of the mesoporous phenolic resin templated by the triblock copolymer ECL4; upon increasing the content of phenolic resin, we observed a mesophase transformation from short-range ordered structure (at 30 wt % phenolic; TEM image in Figure 12p), to cylindrical structures (40−50 wt %; TEM images in Figures 12q,r), to a near-disordered and short/long ordered structure (60 wt %; TEM image in Figure 12s), and finally to a disordered structure (70 wt %; TEM image in Figure 12t). These mesophase transitions are similar to those of the blends of ECL1 and ECL2.

Figure 13 summarizes the phase diagrams of the mesoporous phenolic structures templated by our four ECL triblock

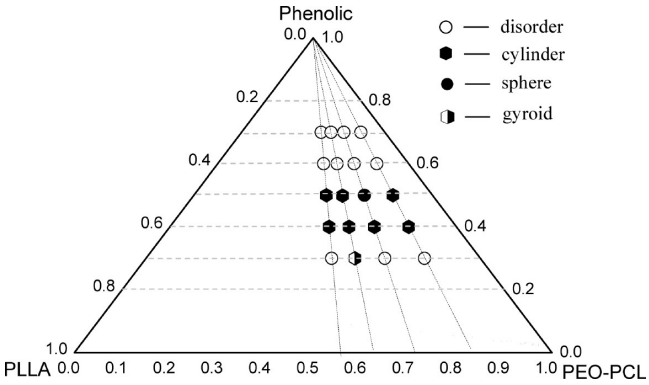

Figure 13. Phase diagram of mesoporous phenolic resins prepared from templating ECL block copolymers. Open circles represent disordered structures; full circles represent regular mesoporous structures.

copolymers, based on the SAXS patterns and TEM images. The presence of phenolic at greater than 60 wt % enhanced the miscibility of the immiscible triblock copolymers based on PEO, PCL, and PLLA. This result is similar to those from many previous studies by Pomposo et al. of PVPh/PEMA/PMMA ternary hydrogen-bonded polymer blends; they have demonstrated that PVPh is miscible with the other components when its content is greater than 65 wt %.[67] To the best of our knowledge, our present paper is the first to report an ABC/D blend system in which the polymer D is miscible with all of the A, B, and C block segments. Here, we combined the PEO and PCL segments into one block, since we could control the molecular weights of these segments in our four triblock copolymers. Figure 13 reveals the existence of a closed-loop mesoporous phenolic resin templated by the ECL triblock copolymers, similar to those obtained from ternary polymer blends in which all three binary pairs (B/A, B/C, A/C) are individually miscible, such as PVPh/PVAc/PEO,[49] SAA/PMMA/PEO,[50] and PVPh/PMMA/PEO,[49] due to the so-called "$\Delta\chi$" and "ΔK" effects in hydrogen-bonded ternary polymer systems. At low phenolic contents (<30 wt %), the system contained insufficient phenolic resin relative to the templating ECL block copolymer and, therefore, formed a disorder structure. At high phenolic contents (>60 wt %), we obtained completely miscible disordered structures because the phenolic OH groups could form hydrogen bonds with all of the PEO, PCL, and PLLA blocks, as confirmed using FTIR spectroscopy. As a result, self-organized mesoporous phenolic resin structures appeared only at phenolic contents of 40−50 wt % because of an intriguing balance between the contents of phenolic and the PEO, PCL, and PLLA blocks. Only one system, phenolic/ECL3 = 30/70, provided a long-range-ordered gyroid structure, at a relatively low phenolic content.

To confirm the mesoporous structures, we recorded their N_2 sorption isotherms; for brevity, we display only those of phenolic/templates = 30/70 in Figure 14. Other N_2 sorption

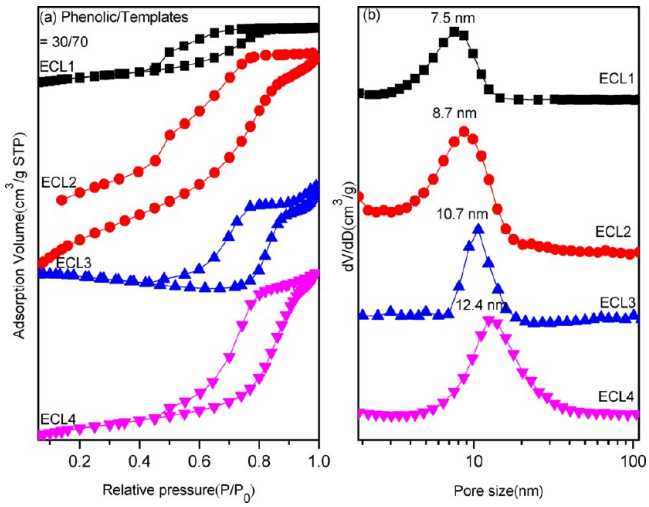

Figure 14. (a) N_2 adsorption/desorption isotherms and (b) pore size distribution curves of mesoporous phenolic structures formed from phenolic/templates = 30/70.

isotherms about phenolic/templates = 40/60 are shown in Figure S7. We observe a representative type IV curve with a sharp capillary condensation step in the relative pressure range from 0.85 to 0.95 as well as a typical H_1-like hysteresis loop at values of P/P_0 from 0.4 to 0.9, suggesting a common mesoporous structure having large, branched, cylindrical pores. The H_1 hysteresis loops for these samples were characteristic of cylindrical mesopores. Based on the Harkins and Jura model,[68] the mean pore size for the mesoporous phenolic templated by the triblock copolymers of ECL, measured from the adsorption branch, was from 7.5 to 12.4 nm. Clearly, the mesoporous sizes were increased with increasing of the PLLA molecular weight in these triblock copolymers. Clearly, according to the position of the first-order scattering peaks from SAXS analyses (Figure 11, d = 16.2, 16.6, 18.5, and 20.9 nm for ELC1, ECL2, ECL3, and ECL4, respectively), the average spacing between the neighboring microdomains, corresponding to the size of the mesoporous domains, systemically increases with increasing of the PLLA

dx.doi.org/10.1021/ma501246j | Macromolecules 2014, 47, 6389−6400

Table 4. Textual Properties of the Mesoporous Phenolic Resins

sample	phenolic/ECL	d^a (nm)	pore size (nm)	$S_{BET}{}^b$ (m^2/g)	$S_M{}^b$ (m^2/g)	pore volume (cm^3/g)	micropore volume (cm^3/g)
phenolic/ECL1	30/70	16.2	7.5	31.4		0.05	
phenolic/ECL2	30/70	16.6	8.7	302.3	106.8	0.31	0.049
phenolic/ECL3	30/70	18.5	10.7	77.7	17.7	0.04	0.008
phenolic/ECL4	30/70	20.9	12.4	49.2		0.14	
phenolic/ECL2	40/60	15.8	7.5	231.6	28.4	0.22	0.011
phenolic/ECL4	40/60	20.2	11.1	37.8	1.5	0.09	

[a]The d-spacing values were calculated by the formula $d = 2\pi/q^*$. [b]S_{BET} and S_M are the total BET surface area and micropore surface area calculated from the t-plots, respectively.

molecular weight in ECL triblock copolymers as shown in Table 4. Unfortunately, we could not measure the mean pore sizes for the samples templated by our ECL triblock copolymers through BET analyses at relatively high phenolic contents (>50 wt %) because the pore volume decreased upon increasing the phenolic content. To the best of our knowledge, this study involves the first fabrication of a long-range-ordered bicontinuous gyroid-type mesoporous phenolic resin, templated by an ABC triblock copolymer, through an evaporation-induced self-assembly strategy. The mesoporous phenolic resin thin films that can be obtained using this approach should be applicable in various fields.

CONCLUSIONS

Employing DSC, TEM, SAXS, and FTIR spectroscopy, we have performed a detailed investigation of the miscibility and hydrogen-bonding interactions, resulting from microphase separation, of self-organized mesoporous phenolic resins from blends containing immiscible PEO-*b*-PCL-*b*-PLLA triblock copolymers as templates. DSC traces and FTIR spectra revealed that phenolic preferred to form hydrogen bonds with the PEO blocks, rather than the PCL and PLLA blocks. At relatively high phenolic contents (>60 wt %), an abundance of OH groups was available for hydrogen bonding with all of the PEO, PCL, and PLLA blocks, and therefore, the blends formed miscible disordered structures; furthermore, phenolic acted as a common solvent in these blend systems. We observed self-organized mesoporous phenolic resin only when the phenolic content was 30−50 wt %—the result of an intriguing balance of the contents of phenolic and the PEO, PCL, and PLLA blocks. At low phenolic contents (<30 wt %), insufficient phenolic resin was present to include the templating ECL triblock copolymers and to form complete mesoporous structures. As a result, a closed-loop mesoporous phenolic resin existed, templated by the ECL block copolymers. TEM images and SAXS analyses indicated that different compositions of phenolic resulted in different mesoporous structures, mediated by the formation of hydrogen bonds.

ASSOCIATED CONTENT

Supporting Information

Figures S1−S7. This material is available free of charge via the Internet at http://pubs.acs.org.

AUTHOR INFORMATION

Corresponding Author

*E-mail kuosw@faculty.nsysu.edu.tw; Tel 886-7-5252000 ext 4079; Fax 886-7-5254099 (S.-W.K.).

Notes

The authors declare no competing financial interest.

ACKNOWLEDGMENTS

This study was supported financially by the Ministry of Science and Technology, Republic of China, under Contracts MOST 100-2221-E-110-029-MY3 and MOST 102-2221-E-110-008-MY3. We thank Mr. Hsien-Tsan Lin of the Regional Instruments Center, National Sun Yat-Sen University, for help with the TEM experiments.

REFERENCES

(1) Rodriguez-Hernandez, J.; Checot, F.; Gnanou, Y.; Lecommandoux, S. *Prog. Polym. Sci.* **2005**, *30*, 691−724.
(2) Hamley, I. U. *The Physics of Block Copolymers*; Oxford University Press: Oxford, UK, 1998.
(3) Foerster, S.; Antonietti, M. *Adv. Mater.* **1998**, *10*, 195−217.
(4) Hadjichristidis, N.; Pispas, S.; Floudas, G. A. *Block Copolymers Synthetic Strategies, Physical Properties, and Applications*; John Wiley & Sons: Hoboken, NJ, 2003.
(5) Han, Y. K.; Pearce, E. M.; Kwei, T. K. *Macromolecules* **2000**, *33*, 1321−1329.
(6) Zhao, J. Q.; Pearce, E. M.; Kwei, T. K. *Macromolecules* **1997**, *30*, 7119−7126.
(7) Kosonen, H.; Ruokolainen, J.; Nyholm, P.; Ikkala, O. *Polymer* **2001**, *42*, 9481−9486.
(8) Kosonen, H.; Ruokolainen, J.; Nyholm, P.; Ikkala, O. *Macromolecules* **2001**, *34*, 3046−3069.
(9) Dobrosielska, K.; Wakao, S.; Takano, A.; Matsushita, Y. *Macromolecules* **2008**, *41*, 7695−7698.
(10) Dobrosielska, K.; Wakao, S.; Suzuki, J.; Noda, K.; Takano, A.; Matsushita, Y. *Macromolecules* **2009**, *42*, 7098−7102.
(11) Chen, S. C.; Kuo, S. W.; Jeng, U. S.; Chang, F. C. *Macromolecules* **2010**, *43*, 1083−1092.
(12) Hameed, N.; Guo, Q. *Polymer* **2008**, *49*, 922−933.
(13) Hameed, N.; Guo, Q. *Macromolecules* **2008**, *41*, 7596−7605.
(14) Salim, N. V.; Hanley, T.; Guo, Q. *Macromolecules* **2010**, *43*, 7695−7704.
(15) Salim, N. V.; Hameed, N.; Guo, Q. *J. Polym. Sci., Part B: Polym. Phys.* **2009**, *47*, 1894−1905.
(16) Hameed, N.; Salim, N. V.; Guo, Q. *J. Chem. Phys.* **2009**, *131*, 214905.
(17) Lee, H. F.; Kuo, S. W.; Huang, C. F.; Lu, J. S.; Chan, S. C.; Wang, C. F.; Chang, F. C. *Macromolecules* **2006**, *39*, 5458−5465.
(18) Chen, W. C.; Kuo, S. W.; Jeng, U. S.; Chang, F. C. *Macromolecules* **2008**, *41*, 1401−1410.
(19) Kuo, S. W. *Polym. Int.* **2009**, *58*, 455−464.
(20) Chen, W. C.; Kuo, S. W.; Lu, C. H.; Chang, F. C. *Macromolecules* **2009**, *42*, 3580−3590.
(21) Lin, I. H.; Kuo, S. W.; Chang, F. C. *Polymer* **2009**, *50*, 5276−5287.
(22) Hillmyer, M. A.; Lipic, P. M.; Hajduk, D. A.; Almdal, K.; Bates, F. S. *J. Am. Chem. Soc.* **1997**, *119*, 2749−2750.
(23) Lipic, P. M.; Bates, F. S.; Hillmyer, M. A. *J. Am. Chem. Soc.* **1998**, *120*, 8963−8970.
(24) Gong, W.; Zeng, K.; Wang, L.; Zheng, S. *Polymer* **2008**, *49*, 3318−3326.
(25) Yi, F.; Zheng, S.; Liu, T. *J. Phys. Chem. B* **2009**, *113*, 1857−1868.

(26) Liang, C.; Dai, S. *J. Am. Chem. Soc.* **2006**, *128*, 5316−5317.
(27) Liang, C.; Hong, K.; Guiochon, G. A.; Mays, J. W.; Dai, S. *Angew. Chem., Int. Ed.* **2004**, *43*, 5785−5789.
(28) Zhuang, X.; Wan, Y.; Feng, C. M.; Shen, Y.; Zhao, D. Y. *Chem. Mater.* **2009**, *21*, 706−716.
(29) Yu, C. Z.; Fan, J.; Tian, B. Z.; Zhao, D. Y. *Chem. Mater.* **2004**, *16*, 889−898.
(30) Deng, Y. H.; Yu, T.; Wan, Y.; Shi, Y. F.; Meng, Y.; Gu, D.; Zhang, L. J.; Huang, Y.; Liu, C.; Wu, X. J.; Zhao, D. Y. *J. Am. Chem. Soc.* **2007**, *129*, 1690−1697.
(31) Valkama, S.; Nykanen, A.; Kosonen, H.; Ramani, R.; Tuomisto, F.; Engelhardt, P.; ten Brinke, G.; Ikkala, O.; Ruokolainen, J. *Adv. Funct. Mater.* **2007**, *17*, 183−190.
(32) Hu, D.; Xu, Z.; Zeng, K.; Zheng, S. *Macromolecules* **2010**, *43*, 2960−2969.
(33) Li, J. G.; Kuo, S. W. *RSC Adv.* **2011**, *1*, 1822−1833.
(34) Li, J. G.; Lin, Y. D.; Kuo, S. W. *Macromolecules* **2011**, *44*, 9295−9309.
(35) Li, J. G.; Chunag, C. Y.; Kuo, S. W. *J. Mater. Chem.* **2012**, *22*, 18583−18595.
(36) Li, J. G.; Chu, W. C.; Jeng, U. S.; Kuo, S. W. *Macromol. Chem. Phys.* **2013**, *214*, 2115−2123.
(37) Kuo, S. W.; Lin, C. L.; Chang, F. C. *Macromolecules* **2002**, *35*, 278−285.
(38) Kuo, S. W. *J. Polym. Res.* **2008**, *15*, 459−486.
(39) Salim, N. V.; Hameed, N.; Hanley, T. L.; Guo, Q. P. *Soft Matter* **2013**, *9*, 6176−6184.
(40) Zhang, J.; Deng, Y.; Wei, J.; Sun, Z.; Gu, D.; Bongard, H.; Liu, C.; Wu, H.; Tu, B.; Schuth, F.; Zhao, D. *Chem. Mater.* **2009**, *21*, 3996−4005.
(41) Qiang, Z.; Xue, J.; Stein, G. E.; Cavicchi, K. A.; Vogt, B. D. *Langmuir* **2013**, *29*, 8703−8712.
(42) Deng, G.; Qiang, Z.; Lecorchick, W.; Cavicchi, K. A.; Vogt, B. D. *Langmuir* **2014**, *30*, 2530−2540.
(43) (a) Bastakoti, B. P.; Ishihara, S.; Leo, S. Y.; Ariga, K.; Wu, K. C. W.; Yamauchi, Y. *Langmuir* **2014**, *30*, 651−659. (b) Li, Y.; Bastakoti, B. P.; Imura, M.; Hwang, S. M.; Sun, Z.; Kim, J. H.; Dou, S. X.; Yamauchi. *Chem.—Eur. J.* **2014**, *20*, 6027−6032. (c) Suzuki, N.; Imura, M.; Nemoto, Y.; Jiang, X.; Yamauchi, Y. *CrystEngComm* **2011**, *13*, 40−43. (d) Jiang, X.; Suzuki, N.; Bastakoti, B. P.; Wu, K. C. W.; Yamauchi, Y. *Chem.—Asian J.* **2012**, *7*, 1713−1718.
(44) Werner, J. G.; Hoheisel, T. N.; Wiesner, U. *ACS Nano* **2014**, *8*, 731−743.
(45) Li, J. G.; Lin, R. B.; Kuo, S. W. *Macromol. Rapid Commun.* **2012**, *33*, 678−682.
(46) Li, J. G.; Lin, R. B.; Kuo, S. W. *RSC Adv.* **2013**, *3*, 17411−17423.
(47) Kuo, S. W.; Huang, C. F.; Tung, Y. C.; Chang, F. C. *J. Appl. Polym. Sci.* **2006**, *100*, 1146−1164.
(48) Patterson, D. *Polym. Eng. Sci.* **1982**, *22*, 64−73.
(49) Zhang, H.; Bhagwagar, D. E.; Graf, J. F.; Paitner, P. C.; Coleman, M. M. *Polymer* **1994**, *35*, 5379−5397.
(50) Jo, W. H.; Kwon, Y. K.; Kwon, I. H. *Macromolecules* **1991**, *24*, 4708−4712.
(51) Kuo, S. W.; Chan, S. C.; Wu, H. D.; Chang, F. C. *Macromolecules* **2005**, *38*, 4729−4736.
(52) Lin, H. C.; Kuo, S. W.; Huang, C. F.; Chang, F. C. *Macromol. Rapid Commun.* **2006**, *27*, 537−541.
(53) Huang, M. W.; Kuo, S. W.; Wu, H. D.; Chang, F. C.; Fang, S. Y. *Polymer* **2002**, *43*, 2479−2487.
(54) Huang, C. F.; Kuo, S. W.; Lin, F. J.; Huang, W. J.; Wang, C. F.; Chen, W. Y.; Chang, F. C. *Macromolecules* **2006**, *39*, 300−308.
(55) Li, J. G.; Chu, W. C.; Kuo, S. W. *J. Nanosci. Nanotechnol.* **2013**, *13*, 2495−2506.
(56) Chiu, C. Y.; Hsu, W. H.; Yen, Y. J.; Kuo, S. W.; Chang, F. C. *Macromolecules* **2005**, *38*, 6640−6647.
(57) Kuo, S. W.; Huang, C. F.; Chang, F. C. *J. Polym. Sci., Part B: Polym. Phys.* **2001**, *39*, 1348−1359.
(58) Kuo, S. W.; Chan, S. C.; Chang, F. C. *J. Polym. Sci., Part B: Polym. Phys.* **2004**, *42*, 117−128.
(59) Kuo, S. W.; Huang, W. J.; Huang, C. F.; Chan, S. C.; Chang, F. C. *Macromolecules* **2004**, *37*, 4164−4173.
(60) Kuo, S. W.; Liu, W. P.; Chang, F. C. *Macromol. Chem. Phys.* **2005**, *206*, 2307−2315.
(61) Coleman, M. M.; Graf, J. F.; Painter, P. C. *Specific Interactions and the Miscibility of Polymer Blends*; Technomic Publishing: Lancaster, PA, 1991.
(62) Coleman, M. M.; Painter, P. C. *Miscible Polymer Blend-Background and Guide for Calculations and Design*; DEStech Publications, Inc.: Lancaster, PA, 2006.
(63) Zhang, L.; Goh, S. H.; Lee, S. Y. *J. Appl. Polym. Sci.* **1998**, *70*, 811−816.
(64) Chu, W. C.; Li, J. G.; Kuo, S. W. *RSC Adv.* **2013**, *3*, 6485−6498.
(65) Zhong, Z.; Guo, Q. *Polymer* **1997**, *38*, 279−286.
(66) Zhong, Z.; Guo, Q. *J. Polym. Sci., Part A: Polym. Chem.* **1998**, *36*, 401−411.
(67) Pomposo, J. A.; Calahorra, E.; Eguiazabal, I.; Cortazar, M. *Macromolecules* **1993**, *26*, 2104−2110.
(68) Harkin, W. D.; Jura, G. *J. Am. Chem. Soc.* **1944**, *66*, 1366−1373.